Stochastic Spatially-Extended Simulations Predict the Effect of ER Distribution on Astrocytic Microdomain Ca^{2+} Activity

Audrey Denizot
audrey.denizot3@oist.jp
Okinawa Institute of Science and Technology,
Computational Neuroscience Unit
Onna-son, Okinawa, Japan

Corrado Calì
Department of Neuroscience, Neuroscience Institute
Cavalieri Ottolenghi
University of Turin
Turin, Italy

Hugues Berry
INRIA, F-69603
Univ Lyon, LIRIS, UMR5205 CNRS, F-69621
Villeurbanne, France

Erik De Schutter
Okinawa Institute of Science and Technology,
Computational Neuroscience Unit
Onna-son, Okinawa, Japan

ABSTRACT

Astrocytes are cells of the central nervous system that can regulate neuronal activity. Most astrocyte-neuron communication occurs at so-called tripartite synapses, where calcium signals are triggered in astrocytes by neuronal activity, resulting in the release of neuro-active molecules by the astrocyte. Most astrocytic Ca^{2+} signals occur in very thin astrocytic branchlets, containing low copy number of molecules, so that reactions are highly stochastic. As those sub-cellular compartments cannot be resolved by diffraction-limited microscopy techniques, stochastic reaction-diffusion computational approaches can give crucial insights on astrocyte activity. Here, we use our stochastic voxel-based model of IP_3R-mediated Ca^{2+} signals to investigate the effect of the distance between the synapse and the closest astrocytic endoplasmic reticulum (ER) on neuronal activity-induced Ca^{2+} signals. Simulations are performed in three dimensional meshes characterized by various ER-synapse distances. Our results suggest that Ca^{2+} peak amplitude, duration and frequency decrease rapidly as ER-synapse distance increases. We propose that this effect mostly results from the increased cytosolic volume of branchlets that are characterized by larger ER-synapse distances. In particular, varying ER-synapse distance with constant cytosolic volume does not affect local Ca^{2+} activity. This study illustrates the insights that can be provided by three-dimensional stochastic reaction-diffusion simulations on the biophysical constraints that shape the spatio-temporal characteristics of astrocyte activity at the nanoscale.

CCS CONCEPTS

• **Applied computing → Life and medical sciences**.

KEYWORDS

computational neuroscience, tripartite synapses, astrocytes, calcium microdomain, reaction-diffusion simulations

NANOCOM '21, September 7–9, 2021, Virtual Event, Italy

ACM ISBN 978-1-4503-8710-1/21/09.
https://doi.org/10.1145/3477206.3477456

ACM Reference Format:
Audrey Denizot, Corrado Calì, Hugues Berry, and Erik De Schutter. 2021. Stochastic Spatially-Extended Simulations Predict the Effect of ER Distribution on Astrocytic Microdomain Ca^{2+} Activity. In *The Eight Annual ACM International Conference on Nanoscale Computing and Communication (NANOCOM '21), September 7–9, 2021, Virtual Event, Italy*. ACM, New York, NY, USA, 5 pages. https://doi.org/10.1145/3477206.3477456

1 INTRODUCTION

Astrocytes, glial cells of the central nervous system, are essential partners of neurons for information processing at so-called tripartite synapses [1]. Astrocytes respond to neuronal activity with changes of intracellular calcium concentration, Ca^{2+} signals, that can trigger the modulation of neuronal communication through the release of neuro-active molecules: gliotransmitters. Astrocytic Ca^{2+} signals are characterized by diverse spatio-temporal properties and differ depending on their localization within the cell. Around 75 % of astrocyte surface belongs to fine branchlets that are unresolved by diffraction-limited microscopy, yet accounting for ≈80 % of Ca^{2+} signals [2]. Ca^{2+} signals are often spatially constricted in those fine branchlets, so that they are hard to detect [14]. Characterizing astrocyte activity at tripartite synapses is thus challenging but crucial to unravel neuron-astrocyte communication in health and disease. Reaction-diffusion computational approaches are an approach of choice for studying astrocyte branchlets, allowing to resolve local Ca^{2+} signals at the nanoscale at the vicinity of neurons.

In this study, we use a stochastic biophysically-detailed model of astrocytic Ca^{2+} signals [3]. Simulations are performed in three spatial dimensions, using STEPS software [7], in idealized fine astrocyte processes geometries. One of the major pathways of Ca^{2+} signals in astrocytes is linked to the Inositol 3-Phosphate receptor (IP_3R) signalling, which induces the release of Ca^{2+} from the endoplasmic reticulum (ER) [16]. IP_3 synthesis is notably activated by the binding of neurotransmitters, released by active presynaptic neurons, to $G_{q/11}$-G-protein-coupled receptors at the membrane of the astrocyte. As electron microscopy [12] and immuno-labelling [9] studies suggest that fine branchlets are characterized by various distances between the astrocytic ER and the closest synapse [12], λ, we tested the influence of the localization of the ER within the astrocytic process on local Ca^{2+} activity. We use our model of IP_3R-mediated

Ca^{2+} signals [3] to test the effect of λ on neuronal activity-induced Ca^{2+} peak characteristics. We show that Ca^{2+} activity decreases rapidly as λ increases, which results from the increased branchlet cytosolic volume with λ. This study illustrates how spatial parameters, such as the distribution of Ca^{2+} stores, can influence neuronal activity-induced Ca^{2+} signals in astrocytes at tripartite synapses.

2 METHODS

2.1 Reaction-diffusion simulations

To investigate the effect of astrocytic ER-synapse distance, λ, on Ca^{2+} dynamics in fine branchlets, characterized by low volumes, voxel-based reaction-diffusion simulations were performed using STEPS stoftware [8]. IP_3R-dependent Ca^{2+} signaling pathway was implemented. Experimentally, Ca^{2+} signals are monitored by using Ca^{2+} indicators, that fluoresce when bound to Ca^{2+} ions. Those indicators thus act as Ca^{2+} buffers and interfere with intracellular Ca^{2+} signaling. In order to allow the comparison of simulation and experimental data, the Ca^{2+} indicator GCaMP6s was added in the cytosol of a subset of simulations, referred to as "GCaMP", which allowed to monitor the concentration of Ca^{2+}-bound fluorescing GCaMP6s molecules. In order to measure the concentration of free Ca^{2+} ions in the absence of Ca^{2+} indicators, which cannot be performed experimentally, a subset of simulations, referred to as "No-GCaMP", did not contain any fluorescent Ca^{2+} indicator. The kinetic scheme and parameter values used in this study have been described in our previous work [3] (code available at http://modeldb.yale.edu/247694).

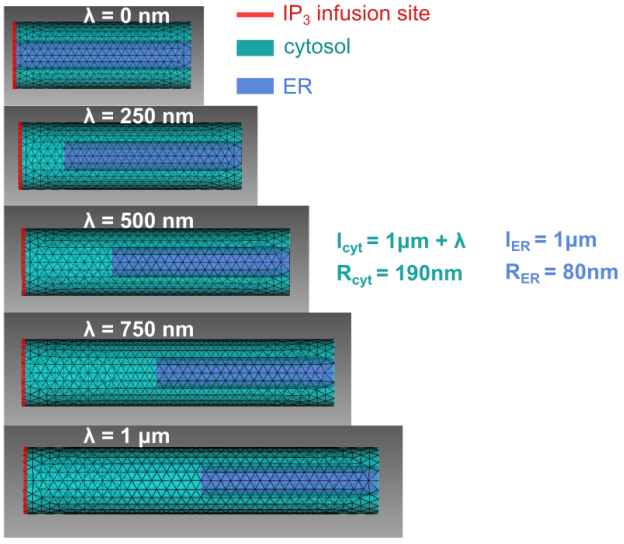

Figure 1: Geometries of fine astrocyte branchlets used in this study. Geometries with various ER-synapse distances were designed. Branchlet morphology consists in a cylinder of radius R_{cyt} = 190 nm radius and of length L_{cyt} = 1μm+λ, containing a cylindrical ER of length L_{ER}=1 μm and radius R_{ER}=80 nm. IP_3 is infused at stimulation time, t=2 s, in the tetrahedra located at the tip of the branchlet (red).

Table 1: Characteristics of the astrocytic branchlet meshes used in this study (see Fig 1).

Geom	ER-synapse dist (nm)	V_{cyt} (nm^3)	S_{PM} (nm^2)
$'Cyl'_0$	0	9.02×10^7	1.41×10^6
$'Cyl'_{250}$	250	1.18×10^8	1.71×10^6
$'Cyl'_{500}$	500	1.46×10^8	2.01×10^6
$'Cyl'_{750}$	750	1.73×10^8	2.30×10^6
$'Cyl'_{1000}$	1000	2.01×10^8	2.60×10^6

To investigate the effect of astrocytic ER-synapse distance, idealized astrocyte branchlet geometries were designed with Trelis software (https://www.csimsoft.com/trelis). The meshes correspond to cylinders of various length L_{cyt}= 1$\mu m + \lambda$ and radius R_{cyt}=190 nm, referred to as 'Cyl_λ', with λ=0, 250, 500, 750 or 1000 nm. Those cylinders contain a cylindrical ER of length L_{ER}=1 μm and radius R_{ER}=80 nm, so that the distance between the IP_3 infusion site and the closest ER triangle to it λ varies between λ=0, 250, 500, 750 or 1000 nm (Fig 1). ER surface area is thus constant across geometries: 5.71×10^5 nm^2, ensuring that the number of IP_3Rs, 160, is constant with λ. Therefore, changes of ER-synapse distance λ were obtained by varying the total process length, which was associated with modifications of total cytosolic volume. The cytosolic volume and surface area of the resulting meshes are presented in Table 1. Neuronal stimulation was simulated as an infusion of 25 IP_3 molecules in sub-membranous tetrahedra at the tip of the process (red line in Fig 1), at time t=2s.
For each condition, twenty simulations with different seed values were performed. During each simulation, Ca^{2+} or Ca-GCaMP concentration was monitored, in "No-GCaMP" and "GCaMP" simulations, respectively.

2.2 Data analysis

Automated Ca^{2+} peak detection was performed as described in [3]. Briefly, a peak corresponds to an increase of Ca^{2+} concentration above the peak threshold (see [3] for details) and terminates when Ca^{2+} concentration decreases below peak threshold. Peak duration corresponds to the time during which Ca^{2+} concentration is above peak threshold. Peak amplitude corresponds to the maximum Ca^{2+} concentration reached during that time interval.

3 RESULTS

3.1 Ca^{2+} microdomain activity decreases as the astrocytic ER-synapse distance increases

To investigate the effect of ER-synapse distance on Ca^{2+} peak characteristics in fine processes, we perform simulations within simplified branchlet geometries (Fig 1), in which the ER is positioned at various distances from the neuronal stimulation site. ER-synapse distance varies from λ=0 to 1 μm, in geometries referred to as $'Cyl_0$ - $'Cyl_{1000}$, respectively. To visualize the spatio-temporal characteristics of Ca^{2+} signals, space was discretized into 100 nm-long bins. Consequently, the branchlet mesh was divided into 10, 15 and 20 bins for $'Cyl_0$, $'Cyl_{500}$ and $'Cyl_{1000}$, respectively (Fig 2A).

Fig 2B displays representative spatio-temporal Ca-GCaMP recordings, revealing the variability of astrocyte activity depending on ER-synapse distance.

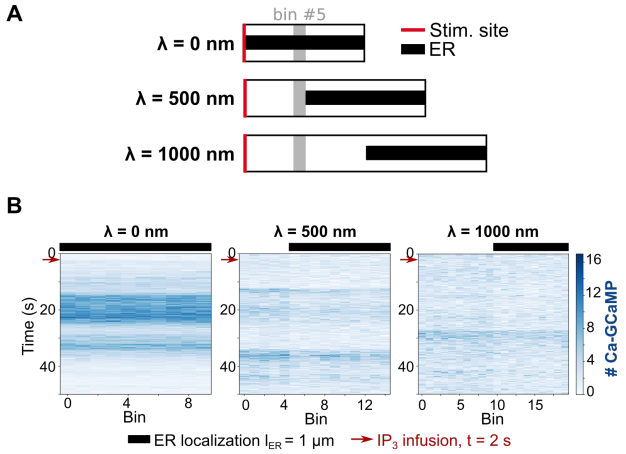

Figure 2: Representative spatio-temporal Ca^{2+} recordings reveal the variability of astrocyte activity depending on ER-synapse distance. (A) Schematic representing the different astrocyte branchlet meshes used in this study. Meshes were characterized by different branchlet length l_{cyt} and constant ER length l_{ER}. IP_3 infusion site, simulating the location of the closest neuronal synapse, is located at the tip of the process and is thus located at various distances to the closest astrocytic ER, λ= 0, 250, 500, 750 and 1000 nm (see Fig 1 and Table 1). In order to display the spatial spread of Ca^{2+} signals within the branchlet, space was discretized into 100 nm-long bins, so that the branchlet was divided into 10, 15 and 20 bins for $'Cyl_0$, $'Cyl_{500}$ and $'Cyl_{1000}$, respectively. Bin #5 is shown in grey. (B) Representative plots illustrating the number of Ca^{2+}-bound GCaMP molecules (Ca-GCaMP) in each bin as a function of time for geometries with λ=0, 500 and 1000 nm, from t=0 s to t=50 s.

IP_3 infusion-induced Ca-GCaMP and Ca^{2+} signals in the whole branchlet qualitatively varied depending on ER-synapse distance λ (Fig 3A). Simulations without Ca^{2+} indicators allowed to predict the effect of λ on free Ca^{2+} signals. Free Ca^{2+} peak amplitude (Fig 3B1), duration (Fig 3B2) and frequency (Fig 3B3) decreased as λ increased (Fig 3B). Overall, our results reveal a strong effect of the ER-synapse distance on Ca^{2+} peak characteristics so that it could contribute to the diversity of Ca^{2+} signals measured experimentally in astrocytes.

3.2 Increased microdomain Ca^{2+} activity as ER-synapse distance decreases results from decreased branchlet cytosolic volume

As cytosolic volume increases with ER-synapse distance λ in geometries $'Cyl_0$ - $'Cyl_{1000}$, we have investigated whether Ca^{2+} peak amplitude, duration and frequency still increase as λ decreases when branchlet cytosolic volume is kept constant. To do so, we

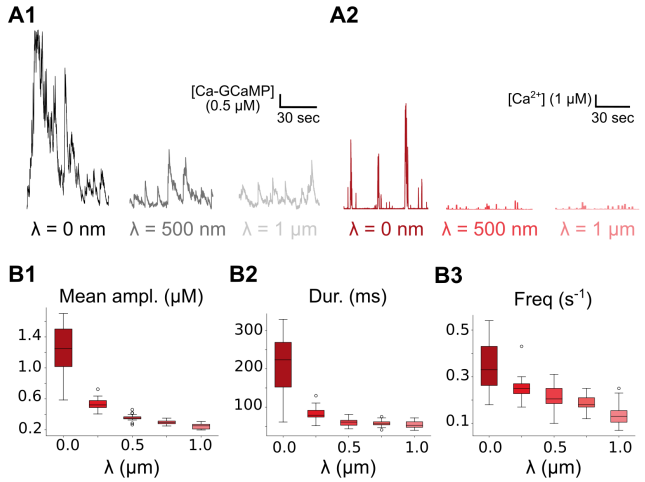

Figure 3: Increased astrocytic ER-synapse distance results in decreased Ca^{2+} microdomain activity. (A1) Representative Ca-GCaMP traces (black) from the "GCaMP" model, for various ER-synapse distances λ=0 (left, dark), 500 (middle) and 1000 nm (right, light) (see Fig 1). (A2) Representative free Ca^{2+} traces (red) from the "No-GCaMP" model, for various ER-synapse distances λ=0 (left, dark), 500 (middle) and 1000 nm (right, light) (see Fig 1). (B) Characteristics of neuronal activity-induced free Ca^{2+} peaks from the "No-GCaMP" model depending on λ. Free Ca^{2+} peak amplitude (B1), duration (B2) and frequency (B3) increase when ER-synapse distance decreases. Data are expressed as box plots from n=20 simulations for each condition.

have performed simulations in the $'Cyl_{1000}$ geometry, in which IP_3 was infused in tetrahedra located at various distances from the closest ER triangle (Fig 4). Ca-GCaMP and Ca^{2+} peaks did not qualitatively vary with λ (Fig 5A). Free Ca^{2+} peak amplitude (Fig 5B1), duration (Fig 5B2) and frequency (Fig 5B3) did not vary with λ. This suggests that the effect of ER-synapse distance on microdomain Ca^{2+} activity reported in Fig 3 results from the increased cytosolic volume of branchlets characterized by larger ER-synapse distances.

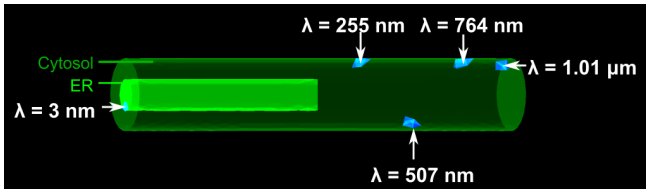

Figure 4: Simulation protocol for simulating neuronal stimulation at various ER-synapse distances with constant branchlet volume. IP_3 was infused in various tetrahedra (blue) in the $'Cyl'_{1000}$ geometry (see Fig 1 and Table 1), located at various distances from the closest ER triangle, resulting in ER-synapse distances λ=3, 255, 507, 764 and 1010 nm. The $'Cyl_{1000}$ geometry is a cylinder of length l_{cyt} = 2 μm.

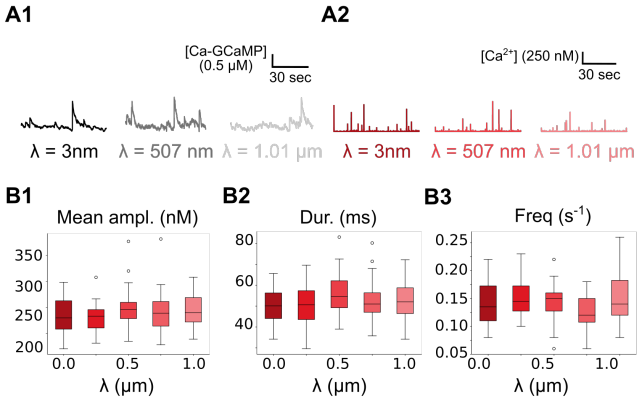

Figure 5: ER-synapse distance with constant branchlet volume does not affect astrocytic Ca^{2+} microdomain activity. (A1) Representative Ca-GCaMP traces (black) from the "GCaMP" model in the $'Cyl'_{1000}$ geometry (Fig 1, for λ=3 (left, dark), 507 (middle) and 1010 nm (right, light). (A2) Representative free Ca^{2+} traces (red) from the "No-GCaMP" model in the $'Cyl'_{1000}$ geometry (see Fig 1, for λ=3 (left, dark), 507 (middle) and 1010 nm (right, light). (B) Characteristics of free Ca^{2+} signals from the "No-GCaMP" model in the $'Cyl'_{1000}$ geometry depending on the location of the IP_3 infusion site (see Fig 4). Free Ca^{2+} peak amplitude (B1), duration (B2) and frequency (B3) did not significantly vary with ER-synapse distance, λ, when branchlet cytosolic volume is kept constant. Data are expressed as box plots from n=20 simulations for each value of λ.

4 DISCUSSION

The endoplasmic reticulum (ER) is an organelle characterized by a very complex morphology, consisting in irregular tubules which can be extremely thin (≈ 15nm), distributed heterogeneously within cells [6]. Because ≈ 75% of astrocyte surface belongs to processes that cannot be resolved by diffraction-limited microscopy [2], their morphology as well as the ultrastructure and distribution of their organelle content remain poorly characterized in live tissue. Electron microscopy studies have been of tremendous importance for characterizing the morphology and distribution of the ER in fixed tissue, revealing the heterogeneous distribution of the ER within astrocyte processes [12, 13]. One study on the hippocampal CA1 region notably suggested that fine processes are practically devoid of ER, which is rather located in thicker processes [12]. In this study, the astrocytic ER was on average 1000 ± 325 nm to the closest postsynaptic density (PSD). Those values however varied drastically from PSD to PSD, so that one of the studied PSD was characterized by an ER-PSD distance of ≈ 400 nm. Further, a recent study performing immuno-labelling of ER-Golgi intermediate compartment (ERGIC) proteins suggested that 32% of synapses in the dorsal hippocampus are contacted by an astrocytic branchlet that contains ERGIC [9]. Together, those observations suggest that the distribution of the ER within processes of a single astrocyte is highly variable and that ER-synapse distance varies drastically depending on the tripartite synapse under study. Here, we investigated the effect of such a heterogeneous distribution of the ER on ER-dependent Ca^{2+} signals. In agreement with previous reports [10], our results suggest that the presence of astrocytic ER at the vicinity of synapses is not mandatory for generating IP_3R-dependent Ca^{2+} signals. Indeed, neuronal activity-induced Ca^{2+} signals were observed in all tested geometries of astrocyte branchlets, including geometries in which the closest astrocytic ER was 1 μm away from the synapse. Our simulations however suggest that a smaller ER-synapse distance is associated to larger Ca^{2+} peak amplitude, duration and frequency. We further propose that this effect is induced by the lower cytosolic volume of branchlets characterized by small ER-synapse distances.

As the structure of the intracellular ER network rearranges constantly via tubule growth, retraction and fusion of adjacent ER membranes, alternating rapidly between tight and loose arrays [5, 11], the ER content of astrocyte branchlets at tripartite synapses is likely to be highly dynamic. According to our simulations, such rapid local changes of ER ultrastructure could influence local Ca^{2+} activity. For example, tubule growth in a branchlet, which would result in a decreased ER-synapse distance and a decreased branchlet cytosolic volume, would result in increased Ca^{2+} peak amplitude, duration and frequency, potentially altering neuron-astrocyte communication locally.

Overall, this study predicts the variability of astrocytic Ca^{2+} signals in microdomains at the vicinity of synapses depending on the distribution of intracellular Ca^{2+} stores. The high spatial resolution of the model allows to characterize the spatio-temporal characteristics of Ca^{2+} signals and allow to predict the dynamics of free Ca^{2+} signals, which cannot be assessed experimentally. Our results illustrate the insights provided by realistic reaction-diffusion simulations in three spatial dimensions on astrocyte activity at the nanoscale. Such models are well suited to investigate spatial effects and the regulation of biochemical interactions in small cellular compartments such as fine astrocytic processes and neuronal dendrites [4, 15]. Exploring such realistic biophysical models of astrocyte Ca^{2+} activity will be crucial to propose plausible mechanisms that regulate local Ca^{2+} activity in microdomains at tripartite synapses.

ACKNOWLEDGMENTS

This work was funded by the Okinawa Institute of Science and Technology Graduate University, Japan, and by JSPS (Japan Society for the Promotion of Science) Standard Postdoctoral Fellowship for Research in Japan (A.D).

REFERENCES

[1] Alfonso Araque, Vladimir Parpura, Rita P. Sanzgiri, and Philip G. Haydon. 1999. Tripartite synapses: glia, the unacknowledged partner. *Trends in Neurosciences* 22, 5 (May 1999), 208–215. https://doi.org/10.1016/S0166-2236(98)01349-6

[2] Erika Bindocci, Iaroslav Savtchouk, Nicolas Liaudet, Denise Becker, Giovanni Carriero, and Andrea Volterra. 2017. Three-dimensional Ca^{2+} imaging advances understanding of astrocyte biology. *Science* 356, 6339 (May 2017), eaai8185. https://doi.org/10.1126/science.aai8185

[3] Audrey Denizot, Misa Arizono, U. Valentin Nägerl, Hédi Soula, and Hugues Berry. 2019. Simulation of calcium signaling in fine astrocytic processes: Effect of spatial properties on spontaneous activity. *PLOS Computational Biology* 15, 8 (Aug. 2019), e1006795. https://doi.org/10.1371/journal.pcbi.1006795

[4] Audrey Denizot, Misa Arizono, Valentin Nägerl, Hugues Berry, and Erik De Schutter. 2021. Astrocyte nanoscale morphology controls Ca2+ signals at tripartite

synapses. *bioRxiv* (Feb. 2021), 2021.02.24.432635. https://doi.org/10.1101/2021.02.24.432635 Publisher: Cold Spring Harbor Laboratory Section: New Results.

[5] Amber R. English and Gia K. Voeltz. 2013. Endoplasmic Reticulum Structure and Interconnections with Other Organelles. *Cold Spring Harbor Perspectives in Biology* 5, 4 (April 2013), a013227. https://doi.org/10.1101/cshperspect.a013227

[6] Rubén Fernández-Busnadiego, Yasunori Saheki, and Pietro De Camilli. 2015. Three-dimensional architecture of extended synaptotagmin-mediated endoplasmic reticulum–plasma membrane contact sites. *Proceedings of the National Academy of Sciences* 112, 16 (April 2015), E2004–E2013. https://doi.org/10.1073/pnas.1503191112

[7] Iain Hepburn. 2013. STEPS: STochastic Engine for Pathway Simulation. In *Encyclopedia of Computational Neuroscience*, Dieter Jaeger and Ranu Jung (Eds.). Springer New York, New York, NY, 1–4. https://doi.org/10.1007/978-1-4614-7320-6_262-7

[8] Iain Hepburn, Weiliang Chen, Stefan Wils, and Erik De Schutter. 2012. STEPS: efficient simulation of stochastic reaction–diffusion models in realistic morphologies. *BMC Systems Biology* 6, 1 (2012), 36. https://doi.org/10.1186/1752-0509-6-36

[9] Noémie Mazaré, Marc Oudart, Julien Moulard, Giselle Cheung, Romain Tortuyaux, Philippe Mailly, David Mazaud, Alexis-Pierre Bemelmans, Anne-Cécile Boulay, Corinne Blugeon, Laurent Jourdren, Stéphane Le Crom, Nathalie Rouach, and Martine Cohen-Salmon. 2020. Local Translation in Perisynaptic Astrocytic Processes Is Specific and Changes after Fear Conditioning. *Cell Reports* 32, 8 (Aug. 2020), 108076. https://doi.org/10.1016/j.celrep.2020.108076

[10] Pavel Montes de Oca Balderas and Horacio Montes de Oca Balderas. 2018. Synaptic neuron-astrocyte communication is supported by an order of magnitude analysis of inositol tris-phosphate diffusion at the nanoscale in a model of peri-synaptic astrocyte projection. *BMC Biophysics* 11 (Feb. 2018), 3. https://doi.org/10.1186/s13628-018-0043-3

[11] Jonathon Nixon-Abell, Christopher J. Obara, Aubrey V. Weigel, Dong Li, Wesley R. Legant, C. Shan Xu, H. Amalia Pasolli, Kirsten Harvey, Harald F. Hess, Eric Betzig, Craig Blackstone, and Jennifer Lippincott-Schwartz. 2016. Increased spatiotemporal resolution reveals highly dynamic dense tubular matrices in the peripheral ER. *Science* 354, 6311 (Oct. 2016), aaf3928. https://doi.org/10.1126/science.aaf3928

[12] Ilya Patrushev, Nikolay Gavrilov, Vadim Turlapov, and Alexey Semyanov. 2013. Subcellular location of astrocytic calcium stores favors extrasynaptic neuron-astrocyte communication. *Cell Calcium* 54, 5 (Nov. 2013), 343–349. https://doi.org/10.1016/j.ceca.2013.08.003

[13] Tatjyana Pivneva, Brigitte Haas, Daniel Reyes-Haro, Gregor Laube, Ruediger W. Veh, Christiane Nolte, Galina Skibo, and Helmut Kettenmann. 2008. Store-operated Ca2+ entry in astrocytes: Different spatial arrangement of endoplasmic reticulum explains functional diversity in vitro and in situ. *Cell Calcium* 43, 6 (June 2008), 591–601. https://doi.org/10.1016/j.ceca.2007.10.004

[14] Dmitri A. Rusakov. 2015. Disentangling calcium-driven astrocyte physiology. *Nature Reviews Neuroscience* 16, 4 (April 2015), 226–233. https://doi.org/10.1038/nrn3878

[15] Cory M. Simon, Iain Hepburn, Weiliang Chen, and Erik De Schutter. 2014. The role of dendritic spine morphology in the compartmentalization and delivery of surface receptors. *Journal of Computational Neuroscience* 36, 3 (June 2014), 483–497. https://doi.org/10.1007/s10827-013-0482-4

[16] Rahul Srinivasan, Ben S. Huang, Sharmila Venugopal, April D. Johnston, Hua Chai, Hongkui Zeng, Peyman Golshani, and Baljit S. Khakh. 2015. Ca(2+) signaling in astrocytes from Ip3r2(-/-) mice in brain slices and during startle responses in vivo. *Nature Neuroscience* 18, 5 (May 2015), 708–717. https://doi.org/10.1038/nn.4001